

Topological protection of defect states from semi-chiral symmetry

Charles Poli and Henning Schomerus*

Department of Physics, Lancaster University, Lancaster, LA1 4YB, United Kingdom

Matthieu Bellec, Ulrich Kuhl, and Fabrice Mortessagne†

Université Nice Sophia Antipolis, Laboratoire de Physique de la Matière Condensée, CNRS UMR 7336, 06100 Nice, France

(Dated: December 9, 2015)

Bipartite quantum systems from the chiral universality classes admit topologically protected zero modes at point defects. However, these states are difficult to separate from compacton-like localized states that arise from flat bands, formed if the two sublattices support a different number of sites within a unit cell. Here we identify a natural reduction of chiral symmetry, obtained by coupling sites on the majority sublattice, which gives rise to spectrally isolated point-defect states, topologically characterized as zero modes supported by the complementary minority sublattice. We observe these states in a microwave realization of a dimerized Lieb lattice with next-nearest neighbour coupling, and also demonstrate topological mode selection via sublattice-staggered absorption.

PACS numbers: 03.65.Vf, 05.60.Gg, 42.82.Et

Symmetry-protected zero modes are an ubiquitous feature of quantum systems exhibiting nontrivial topological phases. Besides their possible realization in electronic systems, these zero modes currently attract considerable attention in photonics [1], where they enable robust unidirectional transport [2–5] in analogy to the quantum hall effect and topological insulators [6–12]. More generally, zero modes can be created by topological defects and interfaces [13–18], and display anomalous features [19–22] that can be exploited, e.g., for topological mode selection [23]. In all these settings, the topological considerations invoke a combination of symmetry with the dimensionality of the bulk and the defects [24, 25]. For instance, a two-dimensional system constrained only by conventional time-reversal symmetry is topologically trivial. Corresponding zero modes, spatially localized at line or point defects, are usually not protected. To obtain nontrivial stationary features, these implementations therefore have to break or modify time-reversal symmetry or rely on system designs that display an additional charge-conjugation or chiral symmetry. The latter setting is appealing as chiral symmetries emerge naturally in bipartite lattices [26, 27] and place the systems into the same universality class as represented by superconductors coupled to strong topological insulators [28–30], meaning that they now can support robust zero modes localized at point defects [25] that can carry a fractional charge and display anyonic statistics [31–35].

As another intriguing consequence of the chiral symmetry, many bipartite lattices of interest, such as the Lieb lattice presented in Fig. 1(a), also exhibit flat bands of zero modes supported by one of the two sublattices (the majority sublattice, which contains more sites per unit cell than the complementary minority sublattice) [26, 27]. These flat bands provide a competing source

of (compacton-like) localized states that are degenerate with any point-defect zero modes [36–43], and also modify constraints on the number of band touchings and Dirac points exhibited by the symmetric dispersive bands of propagating states [26, 27, 38–40], as illustrated in Fig. 1(c).

Here, we describe how one can spectrally isolate

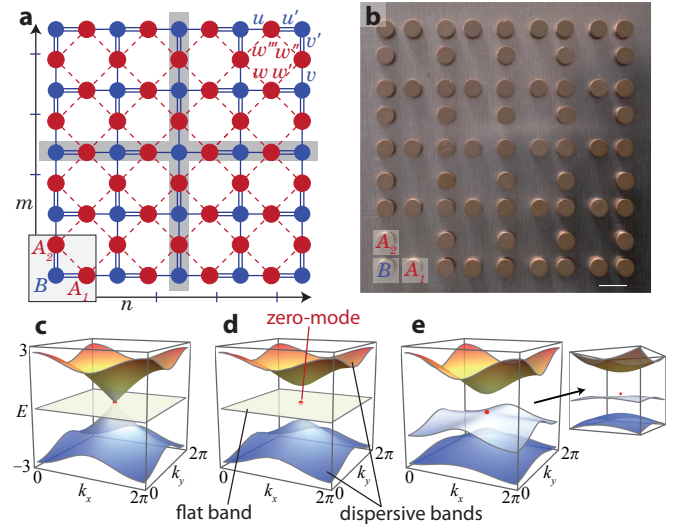


FIG. 1. (a) Lieb lattice with dimerized couplings u, u', v, v' , and next-nearest-neighbour couplings w, w', w'', w''' that reduce the chiral symmetry. This lattice realizes a centered dimerization defect (gray zones). (b) Picture of the experimental microwave realization of the dimerized Lieb lattice. The white bar corresponds to 12 mm. (c-e) Dispersion relation of the infinite system. The zero mode at the M point (red dot) becomes spectrally isolated as one passes from (c) uniform couplings $u = v = u' = v' = 1$ over (d) dimerized couplings $u = v = 4/3, u' = v' = 2/3$, gapping out the extended states, to (e) additional next-nearest-neighbour couplings $w = 0.4, w' = w'' = 0.2, w''' = 0.1$, gapping out the flat band. The inset in (e) shows the vicinity of the M point.

* h.schomerus@lancaster.ac.uk

† fabrice.mortessagne@unice.fr

the point-defect states arising in this setting from the compacton-like states of the flat band. This can be achieved by a well-defined reduction of the chiral symmetry on the majority sublattice, which detunes the compacton-like states due to their anomalous sublattice polarization (imbalanced weight on the sublattices). This situation, which we term semi-chiral symmetry, is realized most naturally in the context of two-dimensional systems, where point-defect states residing on the minority sublattice can be formed when Dirac cones are lifted [see Fig. 1(d)]. The hybridization of the point-defect states with the compacton-like states can then be prevented by breaking the chiral symmetry on the majority sublattice, which moves the flat band away from the chiral symmetry point in the spectrum, as seen in Fig. 1(e). This leaves behind a spatially localized zero mode supported by the minority sublattice, on which the chiral symmetry remains operational.

We first develop a general description of this semi-chiral symmetry, and then focus on its concrete experimental implementation in a dimerized microwave Lieb lattice with next-nearest neighbor couplings [see Fig. 1(b)]. We observe that the point-defect zero mode displays the expected symmetry-protection against a restricted class of disorder, while generic disorder only affects it very weakly. As an application, we demonstrate that the anomalous sublattice polarization of the point-defect state can be exploited for mode selection, which we here achieve by inducing absorption onto the majority sublattice.

Bipartite lattices with semi-chiral symmetry.— Let us first discuss the formation of stable defect states in the general context of two-dimensional bipartite lattices [26, 27]. Such systems consist of two sublattices (A sites and B sites) that are coupled together to result in the following off-diagonal Bloch Hamiltonian [44],

$$h(\mathbf{k}) = \begin{pmatrix} 0 & t_{AB}(\mathbf{k}) \\ t_{BA}(\mathbf{k}) & 0 \end{pmatrix}, \quad E\varphi = h\varphi, \quad \varphi = \begin{pmatrix} \varphi_A \\ \varphi_B \end{pmatrix}. \quad (1)$$

Here $t_{AB}(\mathbf{k}) = t_{BA}^\dagger(\mathbf{k})$ describes the coupling of the A sites to the B sites, whose amplitudes are collected into vectors φ_A and φ_B . The coupling term $t_{AB}(\mathbf{k})$ is thus an $n_A \times n_B$ matrix whose dimensions are given by the count of sublattice sites in the unit cell. We set $n_A \geq n_B$ and identify the A and B sites with the majority and minority sublattice, respectively. Generically, there are then $n_A - n_B$ zero modes for any wavevector \mathbf{k} , given by the solutions of $t_{AB}(\mathbf{k})\varphi_A = 0$ while $\varphi_B = 0$. These dispersionless states constitute the sublattice-polarized flat bands. They are complemented by $2n_B$ dispersive bands of extended states that occur in pairs of opposite energies, while the Bloch wavefunctions carry equal weight on both sublattices. All of these features are intimately linked to the chiral symmetry, $\tau_z h(\mathbf{k}) \tau_z = -h(\mathbf{k})$, where the Pauli matrix τ_z acts in sublattice space; in particular, the sublattice polarization of the zero modes manifests a chiral anomaly.

As \mathbf{k} is varied over the Brillouin zone, the dispersive bands can touch at $E = 0$, meaning that they cross the flat band. This corresponds to situations where the columns of $t_{AB}(\mathbf{k})$ become linearly dependent of each other. We focus on scenarios where this happens at discrete Dirac points $\mathbf{k} = \mathbf{k}_p$ (p integer). If a Dirac point occurs at real \mathbf{k} , one finds two additional zero modes, obtained by the degeneracy of the finite-energy states as $\mathbf{k} \rightarrow \mathbf{k}_p$. Exploiting that these states are related by τ_z , they can be combined into a mode φ_+ on the majority sublattice, as well as a mode φ_- on the minority sublattice—which then obeys $\varphi_{-,A} = 0$, $t_{AB}(\mathbf{k}_p)\varphi_{-,B} = 0$. We now aim to spatially confine and spectrally isolate the state φ_- .

In order to create, as a first step, spatially localized variants of this mode, we have to consider situations where the Dirac point is lifted, so that it lies in the complex \mathbf{k} -plane and describes evanescent zero modes. We identify three important features of these modes — (i) they appear in pairs of distinct wave vectors \mathbf{k}_\pm , (ii) they are supported by opposite sublattices, and (iii) in a finite geometry, only one of them can be compatible with the

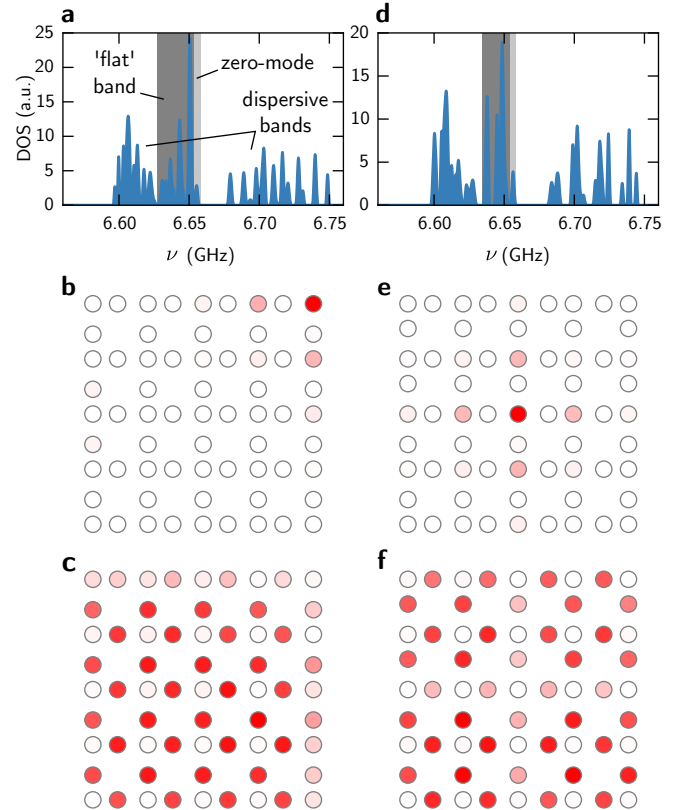


FIG. 2. Experimental results for the microwave realization of the semi-chiral dimerized Lieb lattice, with a defect state localized in the corner (a-c) or in the center (d-f). (a,d) Density of states, with the point-defect zero mode shaded in light gray and the flat band shaded in dark grey. (b,e) Spatial distribution of the zero mode. (c,f) Spatial distribution of the flat band.

boundary conditions. In detail, the mode φ_+ localized on the majority sublattice corresponds to the case of linearly dependent rows of $t_{BA}(\mathbf{k}_+)$, while the mode φ_- localized on the minority sublattice corresponds to linearly dependent rows of $t_{AB}(\mathbf{k}_-)$. As $t_{BA}(\mathbf{k}) = [t_{AB}(\mathbf{k}^*)]^\dagger$, the complex wave vectors \mathbf{k}_+ and $\mathbf{k}_- = \mathbf{k}_+^*$ are distinct and describe states that decay into opposite directions. In a finite system, the mode φ_+ is automatically compatible with the boundary conditions if the system is terminated on the majority sublattice, while for φ_- this is the case for termination on the minority sublattice—the sites just beyond the boundary then lie on the sublattice where the amplitude of the mode vanishes. This zero mode is then exponentially localized around a corner of the system, while its sublattice polarization remains a manifestation of the chiral anomaly. Furthermore, to move this localized zero mode to an arbitrary position within the system, we can create a crossing of line defects that join four regions, in which the mode decays as one moves away from the resulting point defect, as illustrated in Fig. 1(a). The matching conditions are then automatically met if the interface is formed by the appropriate sublattice.

Recall that this zero mode can still hybridize with the flat band. The flat band can now be gapped out by introducing symmetry-breaking terms t_{AA} (but not t_{BB}) into Eq. (1), leading to a Bloch Hamiltonian of the form

$$h(\mathbf{k}) = \begin{pmatrix} t_{AA}(\mathbf{k}) & t_{AB}(\mathbf{k}) \\ t_{BA}(\mathbf{k}) & 0 \end{pmatrix}. \quad (2)$$

Note that this Bloch Hamiltonian fulfills $[\tau_z h(\mathbf{k}) \tau_z]_{BB} = [-h(\mathbf{k})]_{BB}$, which we take as the formal definition of semi-chiral symmetry. While the final configuration does not exhibit a global chiral symmetry, the symmetry is thus still operational on the minority sublattice, and if the point-defect mode was localized on this sublattice neither its wavefunction nor its energy are affected. This then leaves behind a spectrally isolated and spatially localized zero mode supported by the minority sublattice.

Realization of robust point-defect states in a modified Lieb lattice.— The regular Lieb lattice [27] consists of a square sublattice B, with additional sites A_1 and A_2 (forming the A sublattice) placed into the unit cell [gray rectangle in Fig. 1(a)] so that they subdivide each horizontal or vertical edge. This regular lattice has recently been realized in photonic lattices, allowing to directly observe the compacton-like states [36, 37]. Fig. 1(a) shows a dimerized version of the Lieb lattice (with a central defect obtained as discussed below), and Fig. 1(b) its experimental implementation. This consists of an array of 65 microwave cylindrical resonators (5 mm height, 8 mm diameter) made of ZrSnTiO (refractive index 6), placed between two metallic plates [top plate not shown in Fig. 1(b)]. The resonators possess a bare resonance at $\nu = 6.65$ GHz, which is well isolated within a large frequency interval, and are coupled via the evanescent field, with a distance-dependence that has been characterized in detail in Refs. [45, 46]. Via a movable loop-antenna, the reflected signal is measured over a given frequency

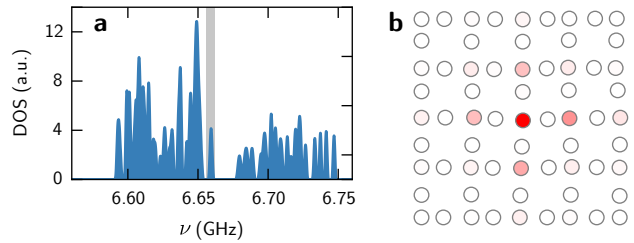


FIG. 3. Experimental results for a disordered dimerized Lieb lattice with a central defect state. Here the disorder fulfills the condition Eq. (3). (a) Density of states, with the point-defect zero mode shaded in light gray. (b) Spatial distribution of the zero mode.

range using a vectorial network analyzer, which gives access to the local and total density of states [46]. The dominant coupling is between nearest neighbors (u, u', v, v'), but next-nearest neighbor couplings of sites on the A sublattice [represented by w, w', w'' and w''' in Fig. 1(a)] are appreciable, while direct couplings on the B sublattice are negligible.

Figures 1(c-e) show the predicted evolution of the band structure with the couplings, obtained by diagonalizing the corresponding Bloch Hamiltonian [44]. Fig. 1(c) corresponds to the situation of a regular Lieb lattice with uniform couplings $u = v = u' = v' = 1$ and $w^{(i)} = 0$. The band structure consists of a flat band of states supported by the A sublattice and two dispersive bands of extended states touching at a conical Dirac point, positioned at the M point $\mathbf{K}_0 = (\pi, \pi)$. As shown on Fig. 1(d), by introducing dimerized couplings $u = v = 4/3$, $u' = v' = 2/3$, a gap 2Δ , with $\Delta^2 = (u - u')^2 + (v - v')^2$, opens up between the dispersive bands, while the flat band and the point-defect state remain fixed at zero energy. This corresponds to a virtual Dirac point at $\mathbf{k}_\pm = \mathbf{K}_0 \pm i\mathcal{A}$, with $\mathcal{A} = [\ln(u/u'), \ln(v/v')]$. Additional next-nearest-neighbour couplings $w = 0.4$, $w' = w''' = 0.2$, $w'' = 0.1$ make the flat band dispersive and move it to finite energies, while also breaking the symmetry of the dispersive bands, but do not affect the defect state, as shown in Fig. 1(e). Without further modification, this defect would be localized around the top right corner of system; as illustrated in Fig. 1(a), the defect state can then be moved along the edges and into the bulk by creating dimerization line defects separating regions where the role of u and u' or v and v' are interchanged.

Figure 2 shows the experimental results for configurations where the point defect sits at the corner [Fig. 2(a-c)] or at the center [Fig. 2(d-f)] of the system. Fig. 2(a) and (d) show the corresponding density of states (DOS). In agreement with the scenario described above, the next-nearest neighbor couplings break the symmetry of the extended bands and isolate the zero mode (light gray zone) from the original flat band (dark gray zone), which now spreads over the whole system but remains mainly confined to the A sublattice [Fig. 2(c), (f)]. As expected, the state associated with the spectrally isolated

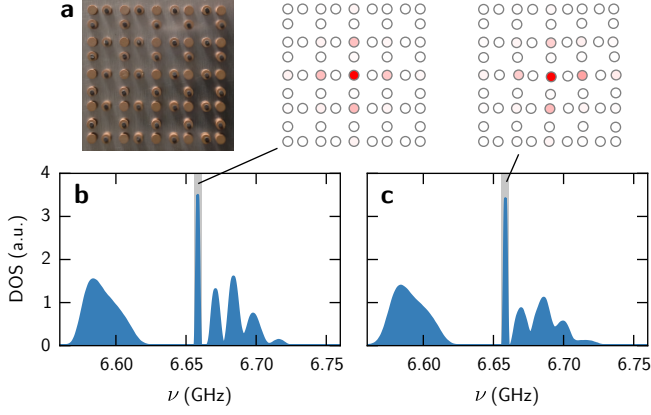


FIG. 4. (a) Picture of the experimental set-up realizing a dimerized Lieb lattice with identical absorption on the A sites, again configured to support a defect state at the center. (b) Density of state of the regular system. (c) Density of state of the disordered system [same configuration as in Fig. 3]. The absorption suppresses the flat-band and extended states, but does not suppress the defect state, which remains localized (insets).

peak displays a spatially localized profile with intensity confined to the B sublattice [Fig. 2(b), (e)].

By construction, this state is insensitive to any disorder in the couplings w, w', w'', w''' . Disorder in the couplings u, u', v, v' modifies the wavefunction, but does not affect its energy or sublattice polarization as long as each plaquette fulfills the constraint

$$u_{nm}v'_{nm}u'_{nm+1}v_{n+1m} = v_{nm}u'_{nm}u_{nm+1}v'_{n+1m}, \quad (3)$$

with couplings enumerated by the unit-cell index of the corresponding A sites [see Fig. 1(a)]. In the continuum limit, where the displacement \mathcal{A} of the virtual Dirac point can be interpreted as an imaginary vectorpotential, this condition amounts to a vanishing pseudomagnetic field induced by the deformation, $\nabla \times \mathcal{A} = 0$.

Fig. 3 (a) shows the experimental DOS of a dimerized Lieb lattice with a central defect and disorder that respects the constraint (3). This disorder was generated on the level of the tight-binding model, where the couplings $u'_{nm} \in [(1-W)u', (1+W)u']$, $v_{nm} \in [(1-W)v, (1+W)v]$, $v'_{nm} \in [(1-W)v', (1+W)v']$ were chosen randomly from box distributions with $W = 0.175$, while the couplings u_{nm} were determined from the constraint (3). These couplings were then translated into a compatible configuration of random displacements, which also introduces disorder into the couplings $w^{(i)}$. In comparison with Fig. 2(d), we see that the disorder is sufficiently strong to mix the extended states, but does not affect the energy of the zero mode, which remains spectrally isolated. Furthermore, the spatial distribution of this mode shown in

Fig. 3(b) exhibits the same localization as observed for the nondisordered lattice in Fig. 2(e). Encouragingly for practical applications, the state remains well localized also for generic disorder, as the spectral isolation of the state suppresses its sensitivity in a perturbative treatment.

Mode selection via staggered absorption.— Our considerations also carry over to an onsite potential on the A sublattice. This includes the choice of an imaginary onsite potential that corresponds to absorption, in generalization of non-hermitian PT -symmetric optics [47–53]. In absence of the next-nearest neighbour couplings, the extended states remain sublattice-balanced for $\gamma < 2\Delta$ and decay according to $\text{Im } E = -\gamma/2$; the states from the flat band decay twice as fast ($\text{Im } E = -\gamma$), while the point-defect state stays pinned at $E = 0$ and thus remains unaffected. In the presence of additional amplification, this correspond to a topological mechanism of mode selection for lasing [20, 21]. In our experiments, we implement the absorption by placing elastomer patches on the top of each A sites [23], thus inducing a uniform absorption on the A sublattice. The selection mechanism can be clearly seen in Fig. 4 where two situations are investigated. Fig. 4(a,b) shows the effect of the absorption on a dimerized Lieb lattice with central defect [same configuration as in Fig. 2(d)], while Fig. 4(c) corresponds to the disordered system in Fig. 3. In both cases, the original flat band and the two dispersive bands are considerably suppressed, while the zero mode is not affected both spectrally as well as in its spatial distribution. Therefore, absorption on the A sublattice can be used to further enhance the spectral isolation of the defect state.

In summary, we showed that a partial breaking of chiral symmetry can be employed to stabilize and isolate point-defect zero modes in bipartite systems with flat bands. Remarkably, the point-defect zero mode resides on the sublattice with the smaller number of sites (the minority sublattice), and thus displays a chiral anomaly with an opposite sign to the flat-band states, which reside on the majority sublattice as expected for zero modes in systems with a chiral anomaly. The flat band states can then be removed by breaking the symmetry on the majority sublattice, without any effects on the point-defect zero mode. As we demonstrated experimentally in a microwave realization of a dimerized Lieb lattice with next-nearest neighbour couplings, the remaining zero mode is spectrally isolated and spatially localized. These features increase the robustness of the state, which is useful for applications in photonic mode shaping and guiding, and also provide a route to mode selection via loss imbalance, which can be extended to laser settings.

This research was supported by EPSRC via Grant No. EP/J019585/1. MB, UK and FM acknowledge helpful contributions from Ioannis Pitsios during the early stage of this work.

-
- [1] L. Lu, J. D. Joannopoulos, and M. Soljačić, *Nat. Photon.* **8**, 821 (2014).
 - [2] Z. Wang, Y. D. Chong, J. D. Joannopoulos, and M. M. Soljačić, *Phys. Rev. Lett.* **100**, 013905 (2008).
 - [3] Z. Wang, Y. Chong, J. Joannopoulos, and M. Soljačić, *Nature* **461**, 772 (2009).
 - [4] M. Hafezi, E. A. Demler, M. D. Lukin, and J. M. Taylor, *Nat. Phys.* **7**, 907 (2011).
 - [5] M. Hafezi, S. Mittal, J. Fan, A. Migdall, and J. M. Taylor, *Nat. Photon.* **7**, 1001 (2013).
 - [6] S. Raghu and F. D. M. Haldane, *Phys. Rev. A* **78**, 033834 (2008).
 - [7] K. Fang, Z. Yu, and S. Fan, *Nat. Photon.* **6**, 782 (2012).
 - [8] A. B. Khanikaev, S. H. Mousavi, W.-K. Tse, M. Kargarin, A. H. MacDonald, and G. Shvets, *Nat. Mater.* **12**, 233 (2013).
 - [9] M. C. Rechtsman, J. M. Zeuner, Y. Plotnik, Y. Lumer, D. Podolsky, F. Dreisow, S. Nolte, M. Segev, and A. Szameit, *Nature* **496**, 196 (2013).
 - [10] M. C. Rechtsman, J. M. Zeuner, A. Tünnermann, S. Nolte, M. Segev, and A. Szameit, *Nat. Photon.* **7**, 153 (2013).
 - [11] J. M. Zeuner, M. C. Rechtsman, S. Nolte, and A. Szameit, *Opt. Lett.* **39**, 602 (2014).
 - [12] S. Mittal, J. Fan, S. Faez, A. Migdall, J. M. Taylor, and M. Hafezi, *Phys. Rev. Lett.* **113**, 087403 (2014).
 - [13] A. Poddubny, A. Miroshnichenko, A. Slobozhanyuk, and Y. Kivshar, *ACS Photonics* **1**, 101 (2014).
 - [14] N. Malkova, I. Hromada, X. Wang, G. Bryant, and Z. Chen, *Opt. Lett.* **34**, 1633 (2009).
 - [15] T. Kitagawa, M. A. Broome, A. Fedrizzi, M. S. Rudner, E. Berg, I. Kassal, A. Aspuru-Guzik, E. Demler, and A. G. White, *Nat. Commun.* **3**, 882 (2012).
 - [16] Y. E. Kraus, Y. Lahini, Z. Ringel, M. Verbin, and O. Zilberberg, *Phys. Rev. Lett.* **109**, 106402 (2012).
 - [17] M. Verbin, O. Zilberberg, Y. E. Kraus, Y. Lahini, and Y. Silberberg, *Phys. Rev. Lett.* **110**, 076403 (2013).
 - [18] R. Keil, J. M. Zeuner, F. Dreisow, M. Heinrich, A. Tünnermann, S. Nolte, and A. Szameit, *Nat. Commun.* **4**, 1368 (2013).
 - [19] M. S. Rudner and L. S. Levitov, *Phys. Rev. Lett.* **102**, 065703 (2009).
 - [20] H. Schomerus and N. Y. Halpern, *Phys. Rev. Lett.* **110**, 013903 (2013).
 - [21] H. Schomerus, *Opt. Lett.* **38**, 1912 (2013).
 - [22] J. M. Zeuner, M. C. Rechtsman, Y. Plotnik, Y. Lumer, S. Nolte, M. S. Rudner, M. Segev, and A. Szameit, *Phys. Rev. Lett.* **115**, 040402 (2015).
 - [23] C. Poli, M. Bellec, U. Kuhl, F. Mortessagne, and H. Schomerus, *Nat. Commun.* **6** (2015).
 - [24] S. Ryu, A. P. Schnyder, A. Furusaki, and A. W. W. Ludwig, *New J. Phys.* **12**, 065010 (2010).
 - [25] J. C. Y. Teo and C. L. Kane, *Phys. Rev. B* **82**, 115120 (2010).
 - [26] B. Sutherland, *Phys. Rev. B* **34**, 5208 (1986).
 - [27] E. H. Lieb, *Phys. Rev. Lett.* **62**, 1201 (1989).
 - [28] Z. M. Hasan and C. L. Kane, *Rev. Mod. Phys.* **82**, 3045 (2010).
 - [29] X.-L. Qi and S.-C. Zhang, *Rev. Mod. Phys.* **83**, 1057 (2011).
 - [30] C. W. J. Beenakker, *Rev. Mod. Phys.* **87**, 1037 (2015).
 - [31] R. Jackiw and C. Rebbi, *Phys. Rev. D* **13**, 3398 (1976).
 - [32] W. P. Su, J. R. Schrieffer, and A. J. Heeger, *Phys. Rev. Lett.* **42**, 1698 (1979).
 - [33] C.-Y. Hou, C. Chamon, and C. Mudry, *Phys. Rev. Lett.* **98**, 186809 (2007).
 - [34] B. Seradjeh, C. Weeks, and M. Franz, *Phys. Rev. B* **77**, 033104 (2008).
 - [35] B. Seradjeh and M. Franz, *Phys. Rev. Lett.* **101**, 146401 (2008).
 - [36] R. A. Vicencio, C. Cantillano, L. Morales-Inostroza, B. Real, C. Mejía-Cortés, St. Weimann, A. Szameit, and M. I. Molina, *Phys. Rev. Lett.* **114**, 245503 (2015).
 - [37] S. Mukherjee, A. Spracklen, D. Choudhury, N. Goldman, P. Öhberg, E. Andersson, and R. R. Thomson, *Phys. Rev. Lett.* **114**, 245504 (2015).
 - [38] D. L. Bergman, C. Wu, and L. Balents, *Phys. Rev. B* **78**, 125104 (2008).
 - [39] D. Green, L. Santos, and C. Chamon, *Phys. Rev. B* **82**, 075104 (2010).
 - [40] J. Mur-Petit and R. A. Molina, *Phys. Rev. B* **90**, 035434 (2014).
 - [41] D. Leykam, O. Bahat-Treidel, and A. S. Desyatnikov, *Phys. Rev. A* **86**, 031805(R) (2012).
 - [42] J. D. Bodyfelt, D. Leykam, C. Danieli, X. Yu, and S. Flach, *Phys. Rev. Lett.* **113**, 236403 (2014).
 - [43] D. Guzmán-Silva, C. Mejía-Cortés, M. A. Bandres, M. C. Rechtsman, S. Weimann, S. Nolte, M. Segev, A. Szameit, and R. A. Vicencio, *New J. Phys.* **16**, 063061 (2014).
 - [44] See the Appendix for a discussion of finite systems, as well as additional details on the dimerized Lieb lattice in the tight-binding description and in the continuum limit.
 - [45] U. Kuhl, S. Barkhofen, T. Tudorovskiy, H.-J. Stöckmann, T. Hossain, L. de Forges de Parny, and F. Mortessagne, *Phys. Rev. B* **82**, 094308 (2010).
 - [46] M. Bellec, U. Kuhl, G. Montambaux, and F. Mortessagne, *Phys. Rev. B* **88**, 115437 (2013).
 - [47] A. Guo, G. J. Salamo, D. Duchesne, R. Morandotti, M. Volatier-Ravat, V. Aimez, G. A. Siviloglou, and D. N. Christodoulides, *Phys. Rev. Lett.* **103**, 093902 (2009).
 - [48] C. E. Rüter, K. G. Makris, R. El-Ganainy, D. N. Christodoulides, M. Segev, and D. Kip, *Nat. Phys.* **6**, 192 (2010).
 - [49] A. Regensburger, C. Bersch, M.-A. Miri, G. Onishchukov, D. N. Christodoulides, and U. Peschel, *Nature (London)* **488**, 167 (2012).
 - [50] L. Feng, Y.-L. Xu, W. S. Fegadolli, M.-H. Lu, J. E. B. Oliveira, V. R. Almeida, Y.-F. Chen, and A. Scherer, *Nat. Mater.* **12**, 108 (2013).
 - [51] T. Eichelkraut, R. Heilmann, S. Weimann, S. Stützer, F. Dreisow, D. N. Christodoulides, S. Nolte, and A. Szameit, *Nat. Commun.* **4**, 2533 (2013).
 - [52] L. Feng, Z. J. Wong, R.-M. Ma, Y. Wang, and X. Zhang, *Science* **346**, 972 (2014).
 - [53] H. Hodaie, M.-A. Miri, M. Heinrich, D. N. Christodoulides, and M. Khajavikhan, *Science* **346**, 975 (2014).

Appendix A: Chiral and semi-chiral symmetry in finite systems

In the main text we focus on Bloch Hamiltonians and take care of boundary conditions by exploiting the anomalous sublattice polarization of the evanescent zero-mode Bloch waves. To prepare a more detailed discussion of the Lieb lattice, we first describe the notions of chiral and semi-chiral symmetry in the context of general (possibly finite and non-periodic) bipartite lattices. Such systems consist of two sublattices (A sites and B sites). The chiral symmetry is realized when these sublattices are coupled together to result in an off-diagonal Hamiltonian, corresponding to real-space tight-binding equations

$$E\psi = H\psi, \quad H = \begin{pmatrix} 0 & T_{AB} \\ T_{BA} & 0 \end{pmatrix}, \quad \psi = \begin{pmatrix} \psi_A \\ \psi_B \end{pmatrix}. \quad (\text{A1})$$

Here $T_{AB} = T_{BA}^\dagger$ describes the coupling of the A sites to the B sites, whose amplitudes are collected in the vectors ψ_A and ψ_B . The Hamiltonian possesses a chiral symmetry, $\tau_z H \tau_z = -H$, where the Pauli matrix τ_z acts in sublattice space. In a finite system with N_A A sites and N_B B sites, T_{AB} is an $N_A \times N_B$ -dimensional matrix. We set $N_A \geq N_B$ and call the A and B sites the majority and minority sublattice, respectively. Generically, the system then possesses $N_A - N_B$ sublattice-polarized zero modes, given by the solutions of the under-determined linear system $T_{BA}\psi_A = 0$ while $\psi_B = 0$ [26, 27]. The chiral symmetry enforces that the remaining $2N_B$ states occur in pairs with energy E and $-E$, and furthermore all possess equal weight on both sublattices, $|\psi_A|^2 = |\psi_B|^2 = 1/2$. The states in each pair are related by τ_z , corresponding to a sign change of the amplitude on the minority sublattice.

As we have shown in the main text, the presence of real or virtual Dirac points allows to increase the zero-mode count by two, with one mode ψ_+ supported by the A sublattice and the other mode ψ_- supported by the B sublattice. This occurs in the general setting when columns of T_{AB} are linearly dependent of each other. The degeneracy of these modes can now again be lifted by introducing terms T_{AA} into the Hamiltonian,

$$H = \begin{pmatrix} T_{AA} & T_{AB} \\ T_{BA} & 0 \end{pmatrix}. \quad (\text{A2})$$

This reduces the chiral symmetry to $[\tau_z H \tau_z]_{BB} = [-H]_{BB}$, which we again can take as the definition of semi-chiral symmetry. This modification does not affect both the energy as well as the wave function of the zero mode ψ_- on the B sublattice, but generically affects all other states—the finite-energy states just as much as the zero modes localized on the A sublattice, including ψ_+ .

Appendix B: Lieb lattice

We here give a very detailed discussion of the formation of the defect state in the dimerized Lieb lattice, first in the tight-binding description and then in the continuum limit.

1. Tight-binding description

The dimerized Lieb lattice with nearest-neighbour couplings is reproduced in Fig. S1. In the tight-binding description, each site $X = A_1, A_2$ or B in a given unit cell provides a basis state $|X_{n,m}\rangle$, with the cells enumerated by a pair of integers n, m . The tight-binding Hamiltonian is then given by

$$\begin{aligned} H = \sum_{nm} & \left[\left(u_{nm}|B_{n,m}\rangle + u'_{nm}|B_{n+1,m}\rangle \right) \langle A_{1;n,m}| \right. \\ & + \left(v_{nm}|B_{n,m}\rangle + v'_{nm}|B_{n,m+1}\rangle \right) \langle A_{2;n,m}| \\ & + \left(w_{nm}|A_{2;n,m}\rangle + w'_{nm}|A_{2;n+1,m}\rangle \right. \\ & \left. + w''_{nm}|A_{2;n+1,m-1}\rangle + w'''_{nm}|A_{2;n,m-1}\rangle \right) \langle A_{1;n,m}| \Big] \\ & + h.c. \end{aligned} \quad (\text{B1})$$

For the infinitely periodic system with $u_{nm} = u$ etc., we can seek solutions in the form of a Bloch wave

$$|\psi(\mathbf{k})\rangle = \sum_{X=A_1,A_2,B} \sum_{nm} e^{i\mathbf{k}\cdot(n,m)} \varphi_X(\mathbf{k}) |X_{n,m}\rangle, \quad (\text{B2})$$

which results in the Bloch eigenvalue problem $E\varphi = h\varphi$,

$$\begin{aligned} h(\mathbf{k}) &= U(k_x)|A_1\rangle\langle B| + V(k_y)|A_2\rangle\langle B| + W(\mathbf{k})|A_1\rangle\langle A_2| + h.c., \\ |\varphi(\mathbf{k})\rangle &= \varphi_{A_1}(\mathbf{k})|A_1\rangle + \varphi_{A_2}(\mathbf{k})|A_2\rangle + \varphi_B(\mathbf{k})|B\rangle, \\ U(k_x) &= u + u'e^{ik_x}, \quad V(k_y) = v + v'e^{ik_y}, \\ W(\mathbf{k}) &= w + w'e^{ik_x} + w''e^{ik_x - ik_y} + w'''e^{-ik_y}, \end{aligned} \quad (\text{B3})$$

where we set the lattice constant $a \equiv 1$.

For the well-studied case of identical nearest-neighbour couplings $u = u' = v = v'$ and $w^{(i)} = 0$, the corresponding band structure consists of a flat band of states $|\varphi_0(\mathbf{k})\rangle \propto V(-k_y)|A_1\rangle - U(-k_x)|A_2\rangle$ localized on the A sublattice, and a conical dispersion relation

$$E^2 = |U(k_x)|^2 + |V(k_y)|^2 \quad (\text{B4})$$

of extended states, with a Dirac point at the M point $\mathbf{K}_0 = (\pi, \pi)$ in the corner of the Brillouin zone. The two degenerate extended states at the Dirac point can be combined into a sublattice-polarized states $|\varphi_+\rangle$, localized on the A sublattice, and $|\varphi_-\rangle = |B\rangle$, where the latter corresponds to a real-space wave function with $|\psi_-\rangle = \sum_{nm} (-1)^{nm} |B_{n,m}\rangle$. This state is compatible with the boundary conditions in finite systems terminated on the B sublattice, as used in the main text and also shown in Fig. S1.

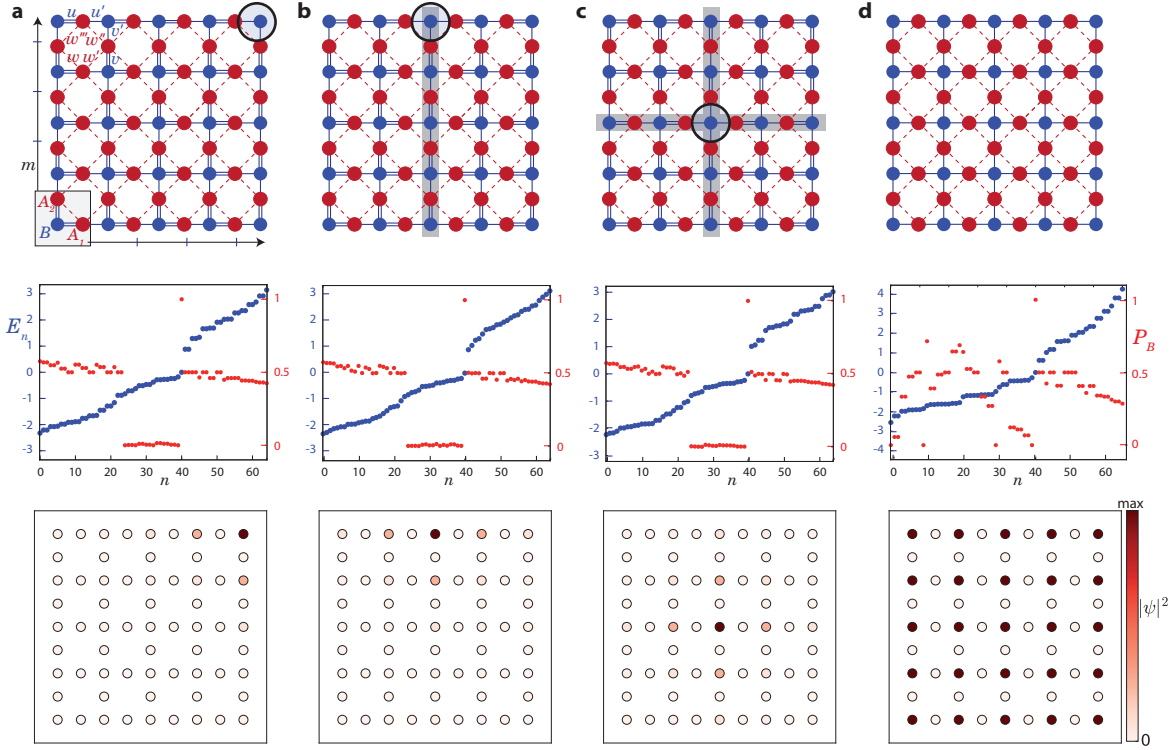


FIG. S1. (a) The top panel shows a finite Lieb lattice with dimerized couplings u, u', v, v' , as well as next-nearest-neighbour couplings w, w', w'', w''' that reduce the chiral symmetry. The circle highlights the site in the top right corner, around which the defect state is localized if $u > u'$ and $v > v'$ (the site is then only coupled by the weak links). The middle row shows the energy levels E_n , in ascending order, and the weights P_B of the eigenstates on the B sublattice, for $u = v = 4/3, u' = v' = 2/3, w = 0.4, w' = w'' = 0.2, w''' = 0.1$. The bottom panel shows the spatial distribution of the isolated zero mode, which is only supported by the B sublattice ($P_B = 1$). (b) The lattice with a vertical dimerization line-defect (gray). Now the defect state is localized around the circled site at the top edge, where again all couplings are weak. (c) The lattice with two dimerization line-defects (gray) that cross in the center of the system, again resulting in a site that only has weak couplings. The defect state is now localized around this central site. (c) Results for the Lieb lattice without dimerization, with $u = v = u' = v' = 1$ and $w = w' = w'' = w''' = 0.5$. The zero mode is now extended, and more fragile to hybridization with the other states in the system.

To see how this state becomes confined by a dimerization pattern (alternating couplings u, u' along the x direction and v, v' along the y direction), we first confirm from Eq. (B4) that this opens a gap 2Δ for the extended states, with $\Delta^2 = E^2(\mathbf{K}_0) = (u - u')^2 + (v - v')^2$. The state $|\varphi_-\rangle$ still survives as a state with a complex wave number $\mathbf{k}_\pm = \mathbf{K}_0 \pm i(\ln u/u', \ln v/v')$, according to the analytical continuation of the Dirac point into the complex plane. The corresponding real-space wavefunction

$$|\psi_-\rangle = \sum_{nm} (-u/u')^n (-v/v')^m |B_{n,m}\rangle \quad (\text{B5})$$

still vanishes on the A sublattice, while on the B sublattice it now has an exponentially varying envelope. In a rectangular finite system, this state remains compatible with the boundary conditions if the system terminates on the B sublattice, and then localizes around a corner of the system. We choose an orientation so that this is the top right corner (this corresponds to $u > u' > 0, v > v' > 0$ and can always be achieved by a rotation of

the system and redefinition of the unit cell), as indicated in Fig. S1(a).

To confirm that the state $|\psi_-\rangle$ can be moved along the edges and into the bulk, we consider line defects separating regions where the role of u and u' or v and v' are interchanged, see Fig. S1(b,c). Along a vertical line defect, we encounter A sites that are coupled by u' both to the right and to the left, while along a horizontal line defect they are coupled by v' both to the bottom and to the top. We denote by $n = m = 0$ the crossing point of two such line defects, or the point where a single line defect meets the upper or right boundary. This results in a point-defect state with real-space wavefunction

$$|\psi_-\rangle = \sum_{nm} (-u/u')^{|n|} (-v/v')^{|m|} |B_{n,m}\rangle, \quad (\text{B6})$$

which now is exponentially localized into all directions. Arbitrary next-to-nearest neighbour couplings $w^{(i)}$ between A_1 and A_2 sites break the symmetry of the extended bands and introduce a dispersion to the flat band,

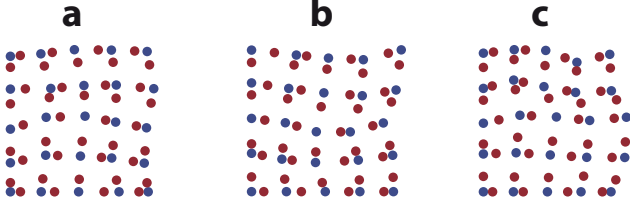


FIG. S2. Disordered Lieb lattices in presence of disorder with strength $W = 0.25$, represented in real space where larger distances d correspond to weaker couplings t . As for the experiment we use an exponential distance-dependence $t \propto \exp(-d/d_0)$, but choose d_0 to make the disorder more visible. Panels (a,b) show configurations that obey the constraint (B7) (generated as described in the main text), while panel (c) shows a configuration with unconstrained disorder.

which moves away to finite energies, as illustrated in Fig. 1 of the main text. However, as a consequence of semi-chiral symmetry, the energy and wave function of the point-defect state (B6) remains unchanged.

These statements are verified by the numerical results in the middle and bottom row of Fig. S1. In each case, we find a spectrally isolated zero mode that is localized on the B sublattice, and exhibits the expected spatial profile (B6).

By construction, the point-defect state (B6) is insensitive to any disorder in the couplings $w_{nm}^{(i)}$. From the condition $T_{AB}\psi_B = 0$, we can further verify that disorder in the couplings $u_{nm}, u'_{nm}, v_{nm}, v'_{nm}$ does not affect the energy or sublattice polarization of the state as long as each plaquette fulfills the constraint

$$u_{nm}v'_{nm}u'_{nm+1}v_{n+1m} = v_{nm}u'_{nm}u_{nm+1}v'_{n+1m}. \quad (\text{B7})$$

Compatible types of disorder include quasi-one-dimensional disorder in which the hoppings u_{nm}, u'_{nm} only depend on the unit-cell index n while the hoppings v_{nm}, v'_{nm} only depend on the unit-cell index m . As described in the main text, the constraint also allows for much richer disorder configurations, some of which are illustrated in Fig. S2.

While we focussed on the implementation of the point-defect state in a photonic setting, we remark that is also interesting to consider this system in an electronic context. In the ground state the single-particle states are then occupied according to the Pauli principle up to a Fermi energy E_F . From a simple counting argument [34], we then find that a uniform charge density at finite filling requires a half-population of the point-defect state. At Fermi energy $E_F = 0^\pm$, the state thus serves as a fractional charge $\pm 1/2$ against a uniform background density on the minority sublattice. This resembles the situation for a Z_4 vortex in a dimerized square lattice (which does not display a flat band), where such states display anyonic statistics [34, 35].

2. Topological characterisation in the continuum limit

An important paradigm of a dimerized system with topologically protected point-defect zero modes is the Su-Schrieffer Heeger (SSH) model [32], which consists of a one-dimensional tight-binding chain with alternating couplings

$$H = \sum_n (u|A_n\rangle + u'|A_{n-1}\rangle)\langle B_n| + h.c. \quad (\text{B8})$$

Here we give an interpretation of the dimerized Lieb lattice as a two-dimensional generalization of the SSH model. This connection is most usefully established in the continuum limit, which sheds further light on the topological features of the system.

For the SSH model, the continuum limit is obtained by a gauge transformation $|A\rangle \rightarrow e^{ik_x/2}|A\rangle$, followed by a gradient expansion in $k_x \rightarrow \pi - i\partial_x$. This results in a massive Dirac Hamiltonian, the Jackiw-Rebbi model [31] with

$$E\psi = H\psi, \quad H = iv_0\sigma_x\partial_x - m\sigma_y, \quad \psi = \begin{pmatrix} \psi_A(x) \\ \psi_B(x) \end{pmatrix}, \quad (\text{B9})$$

where $m = u' - u$ and $v_0 = (u + u')/2$. For constant mass m , the dispersion relation is given by $E^2 = m^2 + v_0^2 k_x^2$. When two regions of opposite mass are joined together, $m(x) = M \operatorname{sgn} x$ with $M > 0$, one finds an exponentially localized defect mode of the form $\psi_A(x) = 0$, $\psi_B(x) \propto \exp(-|x|M/v_0)$.

For the dimerized Lieb lattice, we obtain the continuum limit from the Bloch Hamiltonian (B3) by performing the gauge transformation $|A_1\rangle \rightarrow e^{ik_x/2}|A_1\rangle$, $|A_2\rangle \rightarrow e^{ik_y/2}|A_2\rangle$ and expanding around $\mathbf{k} \rightarrow \mathbf{K}_0 - i\nabla$. We then obtain a massive Dirac Hamiltonian

$$\mathcal{H} = \mathcal{H}_X + \mathcal{H}_Y + \mathcal{H}_{XY}, \quad (\text{B10})$$

$$\mathcal{H}_X = iv_X\lambda_4\partial_x - m_X\lambda_5, \quad (\text{B11})$$

$$\mathcal{H}_Y = iv_Y\lambda_6\partial_y - m_Y\lambda_7, \quad (\text{B12})$$

$$\mathcal{H}_{XY} = m_{XY}\lambda_1 + i\lambda_2(\tilde{v}_X\partial_x + \tilde{v}_Y\partial_y), \quad (\text{B13})$$

where λ_i are the Gell-Mann matrices. The effective velocities are $v_X = (u + u')/2$ and $v_Y = (v + v')/2$, as well as $\tilde{v}_X = (-w - w' + w'' + w''')/2$ and $\tilde{v}_Y = (w - w' - w'' + w''')/2$, while the masses are given by $m_X = u' - u$, $m_Y = v' - v$, $m_{XY} = w - w' + w'' - w'''$.

This model recovers the low-energy part of the band structure. In absence of the couplings $w^{(i)}$, we obtain a flat band of zero modes on the majority sublattice, and dispersive bands with $E^2 = m_X^2 + m_Y^2 + v_X^2 k_x^2 + v_Y^2 k_y^2$. For the system with a vertical dimerization line-defect as in Fig. S1 (b), $m_X(x) = M_X \operatorname{sgn} x$ with $M_X = u - u' > 0$, so that the sign of the mass changes at the interface. This creates a conduction channel within the gap of extended states, described by exponentially confined modes $|\psi\rangle \propto \exp(-|x|M_X/v_X)e^{-ik_y y}[|B(x, y)\rangle + E^{-1}(im_Y - v_Y k_y)|A_2(x, y)\rangle]$, which form two symmetric bands $E^2 =$

$m_Y^2 + v_Y^2 k_y^2$. The channel is thus described by a Jackiw-Rebbi model for the transport along y .

Within this channel, an additional line defect parallel to the x axis should therefore produce a point-defect zero-mode that decays exponentially in all directions. We can verify this directly. For a central dimerization defect as in Fig. S1 (c), the effective masses are given by $m_X(x) = M_X \operatorname{sgn} x$ and $m_Y(y) = M_Y \operatorname{sgn} y$, with $M_X = u - u' > 0$ and $M_Y = v - v' > 0$. While $[\mathcal{H}_X, \mathcal{H}_Y] \neq 0$, we have $([\mathcal{H}_X, \mathcal{H}_Y])_{BB} = 0$, so that the point-defect zero mode on the minority sublattice can be obtained by separation of variables,

$$|\psi_-(x, y)\rangle \propto e^{-\frac{M_X}{v_X}|x|} e^{-\frac{M_Y}{v_Y}|y|} |B(x, y)\rangle. \quad (\text{B14})$$

This indeed corresponds to the continuum limit of the tight-binding solution (B6). We can again verify directly that this state is not affected by the symmetry-breaking terms H_{XY} .

Thus, within the continuum limit the point-defect state

can be associated with a nontrivial background mass pattern in the system. Note that when this mass pattern is smoothed out, the mass-gap order parameter $m_X(\mathbf{r}) + im_Y(\mathbf{r})$ has a non-trivial topology, with a finite winding number as one encircles the origin along a closed loop. This observation establishes an additional connection to systems with charge fractionalization [33].

We conclude by identifying the continuum interpretation of the constraint (B7). In the tight-binding model, the position of the virtual Dirac point can be written as $\mathbf{k}_\pm = \mathbf{K}_0 \pm i\mathcal{A}$, where the displacement $\mathcal{A} = [\ln(u/u'), \ln(v/v')]$ can be interpreted as an imaginary pseudo vector potential (in analogy to the description of strained graphene). We then can rewrite Eq. (B7) as

$$\mathcal{A}_{y;n+1,m} - \mathcal{A}_{y;n,m} = \mathcal{A}_{x;n,m+1} - \mathcal{A}_{x;n,m} \rightarrow \partial_x \mathcal{A}_y = \partial_y \mathcal{A}_x, \quad (\text{B15})$$

therefore $\nabla \times \mathcal{A} = 0$. Thus, the constraint on the disorder can be naturally interpreted as the condition of a vanishing deformation-induced pseudomagnetic field.